MOCVD of BiFeO3 thin films on SrTiO3

Jessica Thery, Catherine Dubourdieu, Thierry Baron, Céline Ternon, Hervé Roussel, Francois Pierre

MOCVD of $BiFeO_3$ Thin Films on $SrTiO_3$**

Jessica Thery, *Catherine Dubourdieu*,* *Thierry Baron*, *Céline Ternon*, *Hervé Roussel*, and *François Pierre*

Bi-Fe-O thin films are grown by liquid-injection metal-organic (MO)CVD on (001) $SrTiO_3$ substrates using two different bismuth precursors, $Bi(tmhd)_3$ and $Bi(mmp)_3$. The precursor $Bi(mmp)_3$ is found to be more effective for Bi incorporation in the films. Epitaxial $BiFeO_3$ films are obtained and no evidence for secondary phases such as Fe_2O_3 or Bi_2O_3 is found by X-ray diffraction (XRD) or transmission electron microscopy (TEM) studies. However, the presence of a multiple binding environment for Fe^{3+} is shown from the X-ray photoelectron spectroscopy (XPS) analyses. Moreover, XPS shows evidence of a Fe^{2+}/Fe^{3+} valence mixed state. A saturation magnetization of 70 emu cm^{-3} is measured. This value is much higher than that reported for the bulk $BiFeO_3$ material. Both the double valence for Fe ions and the enhanced magnetization may originate in the presence of non-fully-oxidized γ-Fe_2O_3.

Keywords: Bismuth iron oxide, Fe valence, MOCVD, Multiferroic materials, Thin films

1. Introduction

Magneto-electric (ME) materials are compounds that present an electric and a magnetic order simultaneously. They can be either ferro-, ferri-, or antiferroelectric and ferro-, ferri-, or antiferromagnetic. They are the subject of intense research, as a coupling between the spontaneous polarization and the spontaneous magnetization offers new promising perspectives for reduced operating power and non-volatile memory applications.[1] One of the first magnetoelectric material discovered, in 1960, was the perovskite $BiFeO_3$ and it is the only one that exhibits multiferroism at room temperature.[2] In bulk form, $BiFeO_3$ is known to be ferroelectric below $T_C \sim 850\,^{\circ}C$ and antiferromagnetic of G-type structure below $T_N \sim 370\,^{\circ}C$.[3] The crystal symmetry (space group R3c) permits a canting of the antiferromagnetic sublattice resulting in a weak ferromagnetism.[4,5] Density functional calculations for unstrained $BiFeO_3$ suggest a local magnetization of around 0.05μB/Fe.[6] However, existence of a superimposed spiral spin structure with an incommensurate long wavelength period of ~62 nm leads to the cancellation of the macroscopic magnetization and thus prevents the observation of the linear ME effect.[2,4,7] Recently, enhanced polarization and magnetization values have been found for $BiFeO_3$ in thin films, leading to a renewal of interest for this compound.[8] Reasons for such an enhancement are still much debated.[9,10]

Many different deposition methods, such as pulsed laser deposition (PLD),[8–14] chemical solution deposition (CSD),[15] liquid phase epitaxy, sol–gel,[16] and sputtering[17,18] have been used for the growth of $BiFeO_3$ films on various substrates. We recently reported the growth of $BiFeO_3$ by MOCVD with $Bi(mmp)_3$ as precursor.[19] Yang et al. have also succeeded using the MOCVD route with $Bi(tmhd)_3$.[20] The very small number of reports related to the MOCVD method as compared to other techniques is most probably due to the difficulty of controlling the stoichiometry of the $BiFeO_3$ films. Bi precursors are indeed not highly volatile, and they are particularly unstable as they can react easily with moisture. For the deposition of Bi-based ferroelectric oxides (such as $Bi_{4-x}La_xTi_3O_{12}$,[21] $Sr_{1-x}Bi_{2+x}Ta_2O_9$,[22] or $Bi_4Ti_3O_{12}$[23]), $Bi(Ph)_3$ and $Bi(tmhd)_3$ appear as the most commonly used Bi-precursors (Ph = phenyl and tmhd = tris 2,2,6,6-tetramethyl-3,5-heptanedionate). Recently, a new bismuth precursor, $Bi(mmp)_3$ (mmp = 1-methoxy-2-methyl-2-propoxide) has been proposed and tested for the MOCVD deposition of bismuth oxide.[24,25] The present work reports on the growth of $BiFeO_3$ thin films by liquid injection MOCVD using $Bi(tmhd)_3$ or $Bi(mmp)_3$ as the bismuth precursor, and $Fe(tmhd)_3$ as the iron precursor. Growth of epitaxial

[*] Dr. C. Dubourdieu, Dr. J. Thery, H. Roussel
Laboratoire des Matériaux et du Génie Physique, UMR CNRS 5628, INPG-Minatec
3 parvis L. Néel, BP257, 38016 Grenoble (France)
E-mail: Catherine.Dubourdieu@inpg.fr
Dr. J. Thery, Dr. T. Baron, Dr. C. Ternon
Laboratoire des Technologies de la Microélectronique, UMR CNRS 5129
17 rue des Martyrs, 38054 Grenoble (France)
F. Pierre
CEA Grenoble
17 rue des Martyrs, 38054 Grenoble (France)

[**] This work has been performed within the European Network of Excellence FAME "Functionalized Advanced Materials and Engineering: Hybrids and Ceramics" (FP6-500159-1). We thank L. Prejbeanau from Spintech laboratory (CEA/CNRS Grenoble) for the VSM measurements and B. Pelissier for XPS expertise.

$BiFeO_3$ films is achieved with both precursors, but a much better control of the stoichiometry is possible with $Bi(mmp)_3$. The films microstructure is studied by means of XRD, XPS, and TEM. The magnetic properties will be also presented.

2. Results and Discussion

2.1. Choice of Precursors

A key issue in CVD is the existence of stable and volatile precursors. For the deposition of complex oxides, metal-organic precursors are preferred to halides, which evaporate at high temperatures. In the case of the liquid injection delivery scheme, the precursor, if a solid, is dissolved in a solvent. An adequate precursor/solvent system must then be found. The liquid precursor should be volatile at temperatures below ~300 °C. In the case of a mixture of precursors, reactions between precursors (such as ligand exchange) must be avoided and the physical properties of both precursors must be close. Since very little information was available, the solubility of distinctive Bi precursors in various solvents has been tested, for molar concentrations varying in the range 0.0001 mol L^{-1} to 0.1 mol L^{-1}. The precursors were dissolved in the solvents in a glove box under an N_2 atmosphere. Table 1 presents some observations on the solubility of common bismuth precursors. It appears that bismuth precursors are not easily soluble in solvents commonly used in liquid injection MOCVD. Moreover, all solutions are quite sensitive to air and moisture exposure (solid formation is observed after such exposure). The $Bi(mmp)_3$ precursor dissolved in octane appeared to be the best candidate as it led to clear solutions for our range of usual concentrations (0.02–0.05 M) for deposition. Moreover, stored solutions in the glove box under N_2 did not show any change after one week (no change in color, no solid formation).

Table 1. Experimental observations on the solubility of Bi precursors in various solvents. Concentrations from 0.1M to 0.0001M have been tested in each case. The solutions that we used are shown in bold. The $Bi(mmp)_3$ solution was received as prepared by Epichem (precursor powder dissolved in octane, 0.05 M).

Chemicals	15 min in ultrasonic bath	Heating at 80 °C + ultrasonic bath	After 48 h (air exposure)
Monoglyme / $Bi(mmp)_3$ Epichem	whitish solution	precipitates	deposits
Monoglyme / $Bi(tmhd)_3$ Epichem	turbid solution	precipitates	deposits
Monoglyme / $Bi(tmhd)_3$ Strem	turbid solution	precipitates	deposits
Monoglyme / $Bi(Ph)_3$ Strem	white deposit	precipitates	deposits
Octane / $Bi(mmp)_3$ Epichem	clear	slightly turbid	deposits
Octane / $Bi(tmhd)_3$ Epichem	slightly turbid	slightly turbid	deposits
Octane / $Bi(tmhd)_3$ Strem	turbid solution	turbid solution	deposits
Octane / $Bi(Ph)_3$ Strem	turbid solution	turbid solution	deposits
Mesitylen / $Bi(tmhd)_3$ Epichem	white precipitates	not tested	deposits
Mesitylen / $Bi(mmp)_3$ Epichem	white precipitates	not tested	deposits
THF/ $Bi(tmhd)_3$ Epichem	yellow flakes	not tested	yellow flakes
Cyclohexan / $Bi(tmhd)_3$ Epichem	white flakes	not tested	white flakes
Pentane / $Bi(tmhd)_3$ Epichem	turbid solution	not tested	precipitates
Heptane / $Bi(tmhd)_3$ Epichem	turbid solution	not tested	precipitates

Figure 1 shows the growth rates for Bi_2O_3 and Fe_2O_3 deposition as a function of substrate temperature, T_s, starting from $Bi(tmhd)_3$, $Bi(mmp)_3$, and $Fe(tmhd)_3$ precursors. The

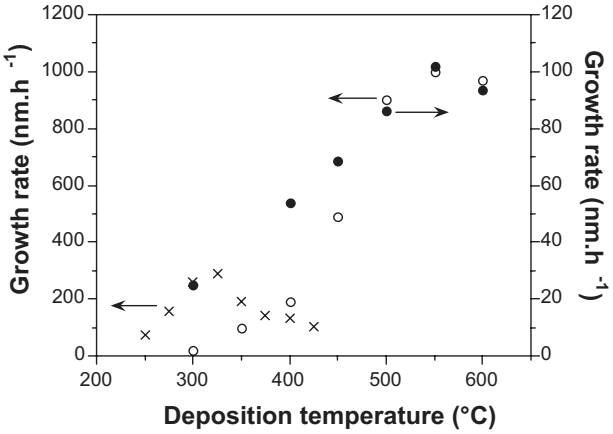

Fig. 1. Comparison of growth rates for $Fe(tmhd)_3$, $Bi(tmhd)_3$, and $Bi(mmp)_3$. Results for $Fe(tmhd)_3$ (filled circles) are from our group, results for $Bi(mmp)_3$ (open circles) are from ref. [25], and results for $Bi(tmhd)_3$ (crosses) are from ref. [26]. The growth rates cannot be compared as experimental set-up and conditions differ in each case.

Fe_2O_3 data are from our group. The Bi_2O_3 data are those reported by S. W Kang et al. for $Bi(tmhd)_3$,[26] and by R. J. Potter et al. for $Bi(mmp)_3$.[25] The growth rates can not be directly compared as different delivery schemes as well as gas flows and pressures were used. However, they give some trends for the different precursors. Iron oxide growth rate appears strongly dependent on T_s, with a maximum around 550 °C. Similarly Bi_2O_3 growth rate with $Bi(mmp)_3$ as precursor shows a maximum around 550 °C. However, the $Bi(tmhd)_3$ precursor presents a quite different behavior, with an optimal growth rate of Bi_2O_3 around 350 °C. This underlines the fact that the decomposition characteristics of $Bi(tmhd)_3$ are very different from those of $Fe(tmhd)_3$. $Bi(mmp)_3$ behaves similarly to $Fe(tmhd)_3$ and seems, thus, more suitable, despite the fact that similar ligands are usually preferred. From these data, T_s was fixed at 550 °C for $BiFeO_3$ deposition.

2.2. Films Deposition Using $Bi(tmhd)_3$

The precursors were dissolved in octane and mixed in solution in varying ratio R_S, where R_S is defined as the molar concentration of $Bi(tmhd)_3$ divided by

the molar concentration of $Fe(tmhd)_3$. Depositions were carried out on (001) $SrTiO_3$ substrates using filtered precursor solutions of concentration 0.05 or 0.02 M; growth parameters are given in Table 2. We injected 4000 droplets of the precursors solution, which corresponds to films

Table 2. Growth conditions of the $BiFeO_3$ films.

Parameters	Conditions
Substrate temperature	550 °C +/- 5 °C
Evaporator temperature	250 °C
Reactor pressure	666 Pa
Ar flow rate	300 sccm
O_2 flow rate	300 sccm
Injection frequency	2 Hz
Injection aperture time	2 ms

thickness of around 200 nm. Figure 2 presents the $\theta/2\theta$ XRD spectra for two R_S values. Textured $BiFeO_3$ (<001> direction perpendicular to the substrate plane) is observed. However, secondary phases are also grown. For $R_S = 0.5$, we note the presence of α-Fe_2O_3 (possibly also γ-Fe_2O_3) and Bi_2O_3 (mostly β-Bi_2O_3 phase but the δ phase may also be present). While increasing the ratio R_S to 2, β-Bi_2O_3 characteristic peaks become predominant, which is consistent with the increase of the $Bi(tmhd)_3$ precursor in solution, while the α-Fe_2O_3 phase disappears. However, repeated experiments at a given R_S value do not lead to reproducible results. We attribute this fact to the poor control of the Bi content, both in solution and in the final gas phase arriving in the deposition zone; both facts prevent controlling the final composition of the deposit. The Bi content in solution is not reproducible due to the poor dissolution of $Bi(tmhd)_3$ in octane. In addition, at 550 °C, the $Bi(tmhd)_3$ precursor decomposes in the gaseous phase. C. Bedoya et al. have shown that the $Bi(tmhd)_3$ precursor stability is critical during its gas-phase transport, and that ligand decomposition is already present at about 80 °C.[27]

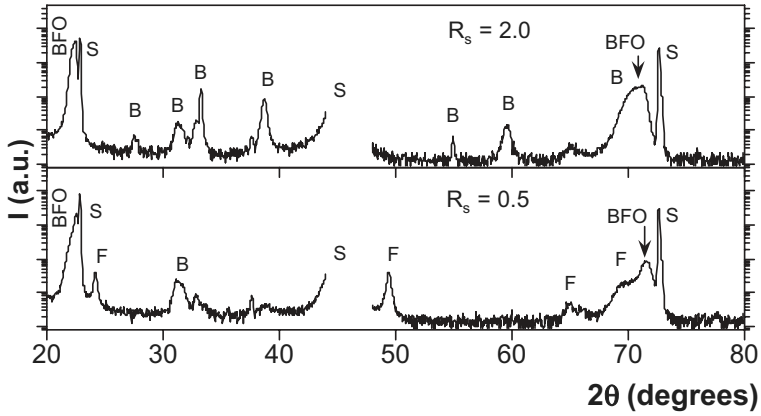

Fig. 2. XRD θ/2θ spectra for films grown on (001) $SrTiO_3$ with $Bi(tmhd)_3$ and $Fe(tmhd)_3$ as bismuth and iron precursors, respectively, for $R_S = 0.5$ (bottom) and $R_S = 2$ (top). The symbol BFO represents $BiFeO_3$, B represents Bi_2O_3, F represents Fe_2O_3, and S represents the $SrTiO_3$ substrate. The 002 $SrTiO_3$ peak has been cut. The peak at $2\theta = 37.6°$ is an artifact of the diffractometer.

Figure 3 shows the morphology of a Bi_2O_3-rich film observed by atomic force microscopy (AFM). Square facetted outgrowths appear on the surface. These crystallites were analyzed by local energy dispersive X-ray spectrometry (EDX), and no iron was found within the accuracy of the measurement, in contrast to the surrounding matrix (containing Bi, Fe, and O). EDX does not give a quantitative measurement of the composition. From the XRD pattern, we can assume that these outgrowths are Bi_2O_3 crystallites. This result is consistent with those of Bea et al.[13] for $BiFeO_3$ films containing Bi_2O_3 and grown by PLD.

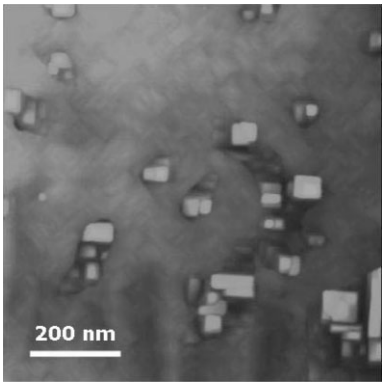

Fig. 3. AFM image for a Bi_2O_3-rich film prepared from the $Bi(tmhd)_3$ precursor. Square facetted Bi_2O_3 grains appear on the surface.

2.3 Film Deposition Using $Bi(mmp)_3$

Filtered precursors solutions with $Bi(mmp)_3$ and $Fe(tmhd)_3$ dissolved in octane were used (0.05 M).The ratio R_S is defined as the molar concentration of $Bi(mmp)_3$ divided by the molar concentration of $Fe(tmhd)_3$. Growth conditions are given in Table 2. Depositions were carried out on (001) Si and (001) $SrTiO_3$. Silicon was used only for compositional analysis. We injected 1500 droplets, which corresponds to films thickness of around 30 nm. Figure 4 presents the $\theta/2\theta$ XRD spectra for three R_S values (on $SrTiO_3$). For $R_S = 1$, we note the presence of Fe_2O_3 phases (α- and possibly γ- and β-Fe_2O_3) and of the perovskite $BiFeO_3$ phase. While increasing the ratio R_S to 1.1, the parasitic phases of the iron oxides disappear. The single phase $BiFeO_3$, textured in the <001> direction, is observed. For $R_S = 1.3$, peaks of Bi_2O_3 appear.

The average films composition was measured using EDX. Due to the limited thickness of the films, standard corrections applied to the data (absorption, fluorescence, Z-number) are no longer valid, and thus the actual composition of the films can not be determined. However, EDX gives a rapid way of comparing samples

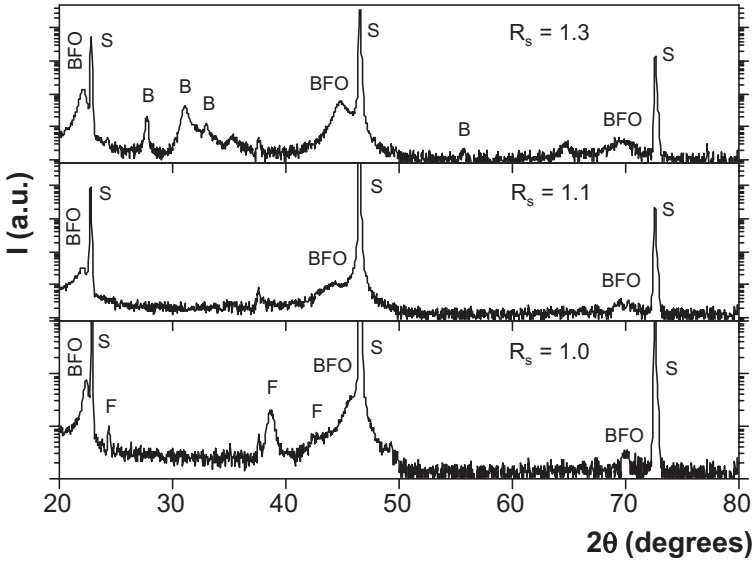

Fig. 4. XRD θ/2θ spectra for films grown on (001) $SrTiO_3$ with $Bi(mmp)_3$ and $Fe(tmhd)_3$ as bismuth and iron precursors, respectively, for three R_S values (1.0, 1.1, and 1.3). The symbol BFO represents $BiFeO_3$, B represents Bi_2O_3, F represents Fe_2O_3, and S represents the $SrTiO_3$ substrate. The peak at $2\theta = 37.6°$ is an artifact of the diffractometer.

and, moreover, it can be calibrated using Rutherford back scattering spectrometry (RBS) as shown later. The average film composition determined from EDX is plotted as a function of the solution composition in Figure 5a for films deposited on $SrTiO_3$ (no significant difference was found for the films deposited on Si). For comparison, we also show the measurements for the films grown using the $Bi(tmhd)_3$ precursor. In both cases, a linear behavior is observed. It is very clear that the $Bi(mmp)_3$ precursor leads to a higher Bi incorporation as compared to $Bi(tmhd)_3$ at the deposition temperature of 550 °C. This is consistent with the results of Figure 1. The cation composition of the films was deduced from RBS measurements. In the case of $SrTiO_3$ substrates, the iron peak overlaps with the substrate contribution and thus the iron content determination is not quite precise. For this reason, films deposited on silicon were used for the composition analyses. Figure 5b presents the measured ratio Bi/Fe in the films as a function of the ratio R_S in the solution. Again a linear behavior is observed, which means that the composition of the films can be controlled by adjusting the composition of the solution. The Bi/Fe stoichiometry of 1 is obtained for a precursor ratio of 1.25 ± 0.05. The oxygen stoichiometry can not be determined and oxygen sub-stoichiometry can not be precluded.

From the XRD spectra, the out-of-plane lattice parameter of stoichiometric films (thickness = 30 nm) is $d_{001} = 0.408$ nm ($c_{bulk} = 0.397$ nm pseudo-cubic). This value is consistent with an in-plane biaxial compressive strain, as expected from the lattice mismatch between $BiFeO_3$ and $SrTiO_3$. XRD spectra for stoichiometric $BiFeO_3$ films show no evidence of any secondary phase, nevertheless this possibility can not be excluded on the single basis of these spectra. Indeed, in the case of a textured growth, peaks of Fe_3O_4 or γ-Fe_2O_3 phases are very close to those of $BiFeO_3$. Moreover, if one assumes that these phases are heteroepitaxially strained, distinction between phases is quite perilous. One can, though, exclude the presence of Fe_3O_4 because of the oxidative growth conditions; for growth of iron oxide films, under the same oxygen partial pressure ($P_{O2} = 333$ Pa), we determined that Fe_3O_4 is oxidized into Fe_2O_3.[28]

TEM and electron diffraction (ED) were performed on selected samples. Figure 6 shows the ED pattern obtained from a cross-section for a 28 nm stoichiometric film. Analyses of the ED patterns reveal that the 001 and 010 reflections have different spacing; $d_{001}/d_{010} \approx 1.02$. Detailed mea-

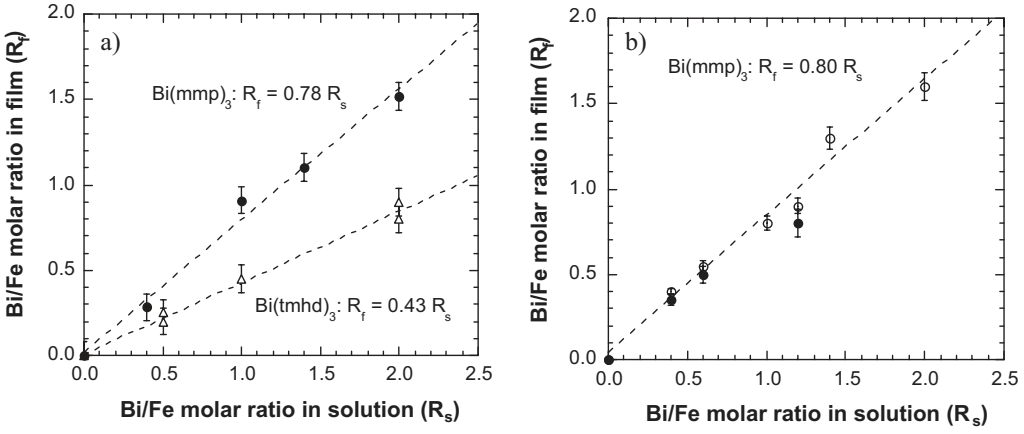

Fig. 5. a) Average cationic films composition measured by EDX as a function of the Bi/Fe ratio in precursor solution for films grown on (001) $SrTiO_3$. Open triangles correspond to the use of $Bi(tmhd)_3$ and closed circles to the use of $Bi(mmp)_3$. b) Average cationic films composition measured by RBS as a function of the Bi/Fe ratio in precursor solution using $Bi(mmp)_3$. Closed and open circles are for depositions on $SrTiO_3$ and Si respectively.

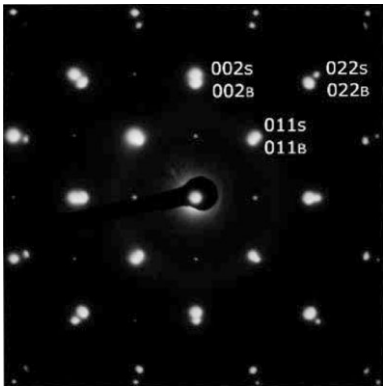

Fig. 6. Electron diffraction pattern of a 28 nm $BiFeO_3$ film grown on (001) $SrTiO_3$ substrate.

sured lattice parameters for this film are; d_{010} ~ 0.394 nm (< $d_{bulk\ 010}$ = 0.397 nm), d_{001} ~ 0.400 nm (> $d_{bulk\ 001}$ = 0.397 nm), and d_{110} ~ 0.285 – 0.289 nm (> $d_{bulk\ 110}$ = 0.282 nm). These values are consistent with XRD spectra and confirm the presence of a compressive biaxial strain in the film plane. No secondary phases were detected from the TEM analyses performed on several area of the films.

We investigated the Fe valence state in our films by measuring the Fe 2p core level XPS spectra. A representative scan of the Fe 2p region is given in Figure 7. Many authors have reported data for the Fe 2p core level spectra of Fe^{2+} and Fe^{3+}.[29–33] In our case, we fitted the Fe $2p_{3/2}$ core level

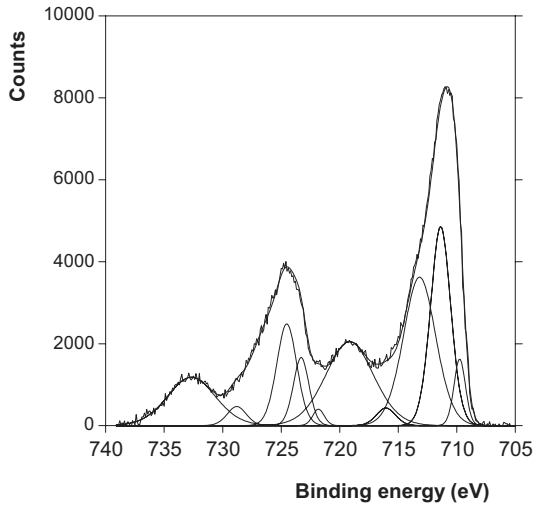

Fig. 7. Fe 2p core level XPS spectra measured on a 30 nm $BiFeO_3$ film and fitted curve with the various contributions.

spectra as follows. The peak at 709.7 eV was attributed to the Fe^{2+} contribution and the peak at 715.9 eV was the corresponding shake-up satellite peak. Peaks at 711.5 and 713.0 eV were attributed to Fe^{3+}. Two peaks are necessary here to fit the Fe^{3+} region; their difference in binding energies (1.5 eV) cannot be attributed to the two distinctive Fe-O distances in $BiFeO_3$ compounds.[34] The two contributions are most probably related to the presence of a secondary phase of iron oxide, in which Fe^{+3} ions occupy both octahedral and tetrahedral sites. Indeed, we found similar contributions in the XPS spectra of γ-Fe_2O_3 films grown at 500 °C on $SrTiO_3$ by the same technique and under the same pressures conditions (P = 666 Pa and P_{O2} = 333 Pa).[28] It is not possible here to identify the nature of the iron oxide phase(s) from the XPS spectra. When iron oxide was deposited on $SrTiO_3$ under the same conditions (T_s = 550 °C, P = 666 Pa, and P_{O2} = 333 Pa), we showed that the films consisted of a mixture of α- and γ-Fe_2O_3.[28] The conditions were too oxidative to obtain Fe_3O_4. The wide peak at 719.0 eV is the corresponding shake-up satellite peak of the Fe^{3+}.

The XPS analyses show that there is evidence of a mixed valence state in our $BiFeO_3$ films. A similar result has been reported for films grown using PLD.[8,10] On the other hand, other groups have reported a single Fe^{3+} valence in their films.[9,11,35] The mixed valence has only been observed for thin films (typically 30–100 nm) and the Fe^{2+} state disappears for thicknesses larger than ~100 nm.[8,10] The origin of the Fe^{2+} ions is not clear. The change in Fe valence could be due to change in Bi valence and/or occurrence of oxygen vacancies. One can also not preclude the presence of Fe^{2+} either in the first stages of the growth of γ-Fe_2O_3 or, conversely, in the core of the γ-Fe_2O_3 precipitates. We have observed, using XPS analysis, a thickness-dependent Fe^{2+}/Fe^{3+} content in γ-Fe_2O_3 films grown on (001) $SrTiO_3$ under a low oxygen partial pressure,[28] with an increasing Fe^{2+} content relatively to Fe^{3+} near the substrate/film interface. On the other hand, it is also possible that the precipitates in the $BiFeO_3$ matrix are not fully oxidized at the core, thus exhibiting a core $Fe_{3-\delta}O_4$/shell γ-Fe_2O_3 structure.

We investigated the magnetic properties of our films using a vibrating sample magnetometer. Figure 8 shows the

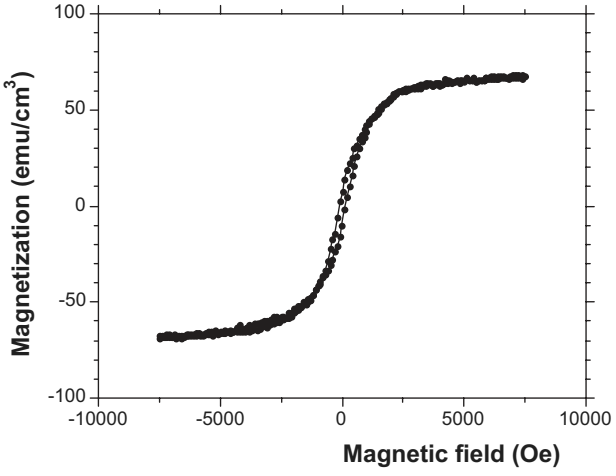

Fig. 8. Magnetization as a function of applied magnetic field for a 30 nm $BiFeO_3$ film showing a saturation magnetization of ~70emu cm^{-3} and a coercive field of ~130 Oe. The magnetic field was applied parallel to the film plane.

corresponding *M-H* curve for a 30 nm epitaxial $BiFeO_3$ film. The magnetic field was applied parallel to the substrate plane. We measure a saturation magnetization of ~70 emu cm^{-3} and a coercive field of ~130 Oe. These observations are similar to those of Wang et al.[8,10] A very low magnetization of ~7 emu cm^{-3} (0.05 μB/Fe) is, however, expected in bulk $BiFeO_3$.[6] Moreover, strained $BiFeO_3$ films prepared using PLD exhibit also a low magnetization (less than 0.06 μB/Fe).[9,35] As suggested by Eerenstein et al.,[9] the enhanced magnetization may arise from the presence of Fe^{2+}. The disappearance of Fe^{2+}, which is experimentally concomitant with a magnetization decrease,[10] strengthens this hypothesis. Bea et al.[35] have shown that the enhanced magnetic properties in their films always arise from the presence of γ-Fe_2O_3 precipitates. In our case, following the XPS analysis, we suggest that our MOCVD films exhibit a γ-Fe_2O_3 secondary phase that gives rise to the enhanced magnetization. The origin of the Fe^{2+} is not clearly determined but may be related to the occurrence of non-fully oxidized γ-Fe_2O_3.

3. Conclusions

In summary, $Bi(mmp)_3$ and $Fe(tmhd)_3$ are shown to be adequate precursors for the growth of $BiFeO_3$ by pulsed liquid injection MOCVD. Films are grown heteroepitaxially on (001) $SrTiO_3$ substrates with in-plane, biaxial compressive strain. Although no secondary phases are found using XRD and TEM, XPS investigations indicate a multiple binding environment for the Fe^{3+} ions, which we attribute to the presence of a secondary phase of iron oxide. XPS analyses also indicate that both Fe^{3+} and Fe^{2+} valences are present in the films. The origin of these Fe^{2+} ions could not be precisely determined. Enhanced magnetization (70 emu cm^{-3}) compared to bulk $BiFeO_3$ is measured. As the link between the occurrence of Fe^{2+} and the deposition conditions is still unclear, investigation of post deposition anneals under O_2 could give further insights into their origin and their role in the physical properties. Finally, from a process point of view, use of heterometallic precursors containing both Bi and Fe should be explored as it could help to improve the control of the stoichiometry of the films.

4. Experimental

$BiFeO_3$ films were grown by liquid injection MOCVD. The liquid injection delivery scheme allows one to control precisely the amount of precursors delivered into the deposition chamber. Moreover, it also permits the evaporation of a single cocktail of several precursors with different characteristics thanks to the flash evaporation of micro-liter droplets. A detailed description of the injection system and of the reactor can be found elsewhere [36]. The reactor was a vertical, quartz tube reactor. Ar was used as a carrier gas and O_2 as an oxidizing agent. Oxygen was mixed with the gaseous reactive species in the evaporator. The substrate temperature (550 °C), the evaporation temperature (250 °C), the total pressure (666 Pa), and the gas flow (300 sccm of Ar and 300 sccm of O_2) were kept constant during the study (P_{O2} = 333 Pa). Injection parameters were fixed at 2 ms for the opening time and 2 Hz for the injection frequency. To induce heteroepitaxial growth, films were grown on (001) $SrTiO_3$ substrates (10 mm × 10 mm^2). Lattice parameters mismatch between both perovskites-type oxides was ~1 %, leading to a compressive biaxial strain in the film plane. The substrates were prepared with a procedure based on the work of Kawasaki et al. in order to have atomically flat and -TiO_2 terminated surfaces [37]. For compositional analysis, films were also grown on (001) silicon substrates (10 mm × 10 mm^2).

XRD (θ/2θ scans) was performed on a Siemens D500 diffractometer equipped with a monochromator and using Cu Kα radiation (λ = 1.5406 Å). EDX was performed on a Philips XL30 SEM using a Tracor spectrometer. For each composition determination, five analyses were acquired and averaged. XPS was performed on a ESCALAB 220i from VG Scientific using a monochromatized Al Kα source ($h\nu$ = 1486.6 eV). A hemispherical electron analyzer was used in fixed pass energy filter mode (20 eV). Energy calibration was performed by positioning the surface carbon contamination peak at 284.8 +/– 0.1 eV. Magnetic measurements were carried out using a vibrating sample magnetometer from ADE. For *M-H* curves, the magnetic field was applied parallel to the substrate plane.

[1] M. Fiebig, *J. Phys. D*: *Appl. Phys.* **2005**, *38*, R123.
[2] Yu. N. Venevtsev, G. Zdhanov, S. Solov'ev, *Sov. Phys. Crystallogr.* **1960**, *4*, 538.
[3] Yu. F. Popov, A. K. Zvezdin, G. P. Vorob'ev, A. M. Kadomtseva, V. A. Murashev, D. N. Rakov, *JETP Lett.* **1993**, *57*, 69.
[4] I. E. Dzyaloshinskii, *J. Phys. Chem. Solids* **1958**, *4*, 241.
[5] I. Sosnowska, T. Peterlin-Neumaier, E. Steichele, *J. Phys. C*: *Solid State Phys.* **1982**, *15*, 4835.
[6] C. Ederer, N. A. Spalding, *Phys. Rev. B* **2005**, *71*, 060401.
[7] I. Sosnowska, M. Loewenhaupt, W. I. F. David, R. M. Ibberson, *Physica B* **1992**, *180-181*, 117.
[8] J. Wang, J. B. Neaton, H. Zheng, V. Nagarajan, S. B. Ogale, B. Liu, D. Viehland, V. Vaithyanathan, D. G. Schlom, U. V. Waghmare, N. A. Spaldin, K. M. Rabe, M. Wuttig, R. Ramesh, *Science* **2003**, *299*, 1719.
[9] W. Eerenstein, F. D. Morrison, J. Do, M. G. Blamire, J. F. Scott, N. D. Mathur, *Science* **2005**, *307*, 1203a.
[10] J. Wang, A. Scholl, H. Zheng, S. B. Ogale, D. Viehland, D. G. Schlom, N. A. Spaldin, K. M. Rabe, M. Wuttig, L. Mohaddes, J. Neaton, U. Waghmare, T. Zhao, R. Ramesh, *Science* **2005**, *307*, 1203b.
[11] K. Y. Yun, M. Noda, M. Okuyama, *Appl. Phys. Lett.* **2003**, *83*, 3981.
[12] K. Y. Yun, M. Noda, M. Okuyama, H. Saeki, H. Tabata, K. Saito, *J. Appl. Phys.* **2004**, *96*, 3399.
[13] H. Bea, M. Bibes, A. Barthélémy, K. Bouzehouane, E. Jacquet, A. Khodan, J.-P. Contour, S. Fusil, F. Wyczisk, A. Forget, D. Lebeugle, D. Colson, M. Viret, *Appl. Phys. Lett.* **2005**, *87*, 072508.
[14] H. Béa, M. Bibes, A. Barthélémy, K. Bouzehouane, A. Khodan, J.-P. Contour, S. Fusil, F. Wyczisk, A. Forget, D. Lebeugle, D. Colson, M. Viret, *Appl. Phys. Lett.* **2005**, *88*, 062502.
[15] S. Iakovlev, C. H. Solterbeck, M. Kuhnke, M. Es-Souni, *J. Appl. Phys.* **2005**, *97*, 094901.
[16] X. Qi, J. Dho, M. Blamire, Q. X. Jia, J.-S. Lee, S. Foltyn, J. L. MacManus-Driscoll, *J. Mag. Mag. Mater.* **2004**, *283*, 415.
[17] Y. H. Lee, C. S.Liang, J. M. Wu, *Electrochem. Solid-State Lett.* **2005**, *8*, F55.
[18] C. Ternon, J. Thery, T. Baron, C. Ducros, F. Sanchette, J. Kreisel, *Thin Solid Films* **2006**, *515*, 481.
[19] J. Thery, T. Baron, C. Dubourdieu, C. Ternon, B. Pelissier, H. Roussel, S. Coindeau, I.-L. Prejbeanu, *Silicon Nitride and Silicon Dioxide Thin Insulating Films and other Emerging Dielectrics VIII* [Eds: R. E. Sah, M. J. Deen, J. Zhang, J. Yota, Y. Kamakura], PV 2005-01 - ISBN 1-56677-459-4, Electrochemical Society, Pennington, NJ **2005**, pp. 498–509
[20] S. Y. Yang, F. Zavaliche, L. Mohaddes-Ardabili, V. Vaithyanathan, D. G. Schlom, Y. J. Lee, Y. H. Chu, M. P. Cruz, Q. Zhan, T. Zhao, R. Ramesh, *Appl. Phys. Lett.* **2005**, *87*, 102903.
[21] S.-W. Kang, S.-W. Rhee, *J. Vac. Sci. Technol. A* **2003**, *21*, 340.
[22] J. F. Roeder, B. C. Hendrix, F. Hintermaier, D. A. Desrochers, T. H. Baum, G. Bhandari, M. Chappuis, P. C. Van Buskirk, C. Dehm, E. Fritsch, N. Nagel, H. Wendt, H. Cerva, W. Hönlein, C. Mazuré, *J. Eur. Ceram. Soc.* **1999**, *19*, 1463.
[23] T. Nakamura, R. Muhammet, M. Shimizu, T. Shiosaki, *Jpn. J. Appl. Phys. Part. 1* **1993**, *32*, 4086.

[24] P. A. Williams, A. C. Jones, M. J. Crosbie, P. J. Wright, J. F. Bickley, A. Steiner, H. O. Davies, T. J. Leedham, G. W. Critchlow, *Chem. Vap. Deposition* **2001**, *7*, 205.
[25] R. J. Potter, P. A. Marshall, J. L. Roberts, A. C. Jones, P. R. Chalker, M. Vehkamäki, M. Ritala, M. Leskelä, P. A. Williams, H. O. Davies, N. L. Tobin, L. M. Smith, *Mater. Res. Soc. Symp. Proc.* **2004**, *784*, 97.
[26] S. W. Kang, S. W. Rhee, *Thin Solid Films* **2004**, *468*, 79.
[27] C. Bedoya, G. G. Condorelli, S. T. Finocchiaro, A. Di Mauro, I. L. Fragala, L.Cattaneo, S. Carella, *Chem. Vap. Deposition* **2005**, *11*, 261.
[28] J. Thery, B. Pelissier, T. Baron, H. Roussel, C. Dubourdieu, unpublished.
[29] P. Mills, J. L. Sullivan, *J. Phys. D*: *Appl. Phys.* **1983**, *16*, 723.
[30] J. F. Moulder, W. F. Stickle, P. E. Sobol, K. D. Bomben, in *Handbook of X-Ray Photoelectron Spectroscopy* (Ed: J. Chastain), Perkin-Elmer Corporation **1992**.
[31] Th. Schedel-Niedrig, W. Weiss, R. Schlögl, *Phys. Rev. B* **1995**, *52*, 17449.
[32] P. Graat, M. A. J. Somers, *Surf. Interf. Anal.* **1998**, *26*, 773.
[33] T. Fujii, F. M. F. de Groot, G. A. Sawatzky, F. C. Voogt, T. Hibma, K. Okada, *Phys. Rev. B* **1999**, *59*, 3195.
[34] F. Kubel, H. Schmid, *Acta Crystallogr. Sect. B: Struct. Sci.* **1990**, *B46*, 698.
[35] H. Bea, M. Bibes, S. Fusil, K. Bouzehouane, E. Jacquet, K. Rode, P. Bencok, A. Barthélémy, *Phys. Rev. B* **2006**, *74*, 020 101(R).
[36] J. P. Sénateur, C. Dubourdieu, F. Weiss, M. Rosina, A. Abrutis, *Adv. Mater. Optics Electron.* **2000**, *10*, 155.
[37] M. Kawasaki, K. Takahashi, T. Maeda, R. Tsuchiya, M. Shinohara, O. Ishiyama, T. Yonesawa, M. Yoshimoto, H. Koinuma, *Science* **1994**, *266*, 1540.